# Assessment of $PrBaCo_2O_{5+\delta} + Sm_{0.2}Ce_{0.8}O_{1.9}$ composites prepared by physical mixing as electrodes of solid oxide fuel cells

Dengjie Chen, Ran Ran, Zongping Shao *

State Key Laboratory of Materials-Oriented Chemical Engineering, College of Chemistry & Chemical Engineering, Nanjing University of Technology, No. 5 Xin Mofan Road, Nanjing 210009, PR China

## ARTICLE INFO

## ABSTRACT

The performance of $PrBaCo_2O_{5+\delta} + Sm_{0.2}Ce_{0.8}O_{1.9}$ (PrBC + SDC) composites as electrodes of intermediate-temperature solid oxide fuel cells is investigated. The effects of SDC content on the performance and properties of the electrodes, including thermal expansion, DC conductivity, oxygen desorption, area specific resistance (ASR) and cathodic overpotential are evaluated. The thermal expansion coefficient and electrical conductivity of the electrode decreases with an increase in SDC content. However, the electrical conductivity of a composite electrode containing 50 wt% SDC reaches 150 S cm$^{-1}$ at 600 °C. Among the various electrodes under investigation, an electrode containing 30 wt% SDC exhibits superior electrochemical performance. A peak power density of approximately 1150 and 573 mW cm$^{-2}$ is reached at 650 and 550 °C, respectively, for an anode-supported thin-film SDC electrolyte cell with the optimal composite electrode. The improved performance of a composite electrode containing 70 wt% PrBC and 30 wt% SDC is attributed to a reduction in the diffusion path of oxygen-ions within the electrode, which is a result of a three-dimensional oxygen-ion diffusion path in SDC and a one-dimensional diffusion path in PrBC.

## 1. Introduction

Solid oxide fuel cells (SOFCs) are high-temperature electrochemical devices that can convert chemical energy to electrical power with high efficiency and low emissions. SOFC single cells are typically composed of a cathode, an anode and an electrolyte, where oxygen reduction reactions occur at the cathode. $La_{0.8}Sr_{0.2}MnO_3$ (LSM) is a state-of-the-art cathode material for high-temperature SOFCs [1,2], which performs well at temperatures between 750 and 1000 °C; the higher temperatures represent the cathode- and electrolyte-supported cells, the lower the anode-supported ones. It is well accepted that the reduction in operating temperatures to the low-to-intermediate temperature range (500–750 °C) would greatly accelerate the wide application of this attractive new technology [3–6]. However, a reduced operating temperature introduces new challenges for the electrodes, electrolytes and fuels. Below 650 °C the SOFC can be operated only either with hydrogen or with another gas but not the typical ones such as natural gas due to carbon deposition.

The active sites for oxygen reduction reaction over a pure electronic conducting electrode are typically located around the triple phase boundary (TPB) regions, where the electrolyte, electrode and gas phase meet [7]. Introduction of an ionic conducting path into the electrode is an effective way to increase TPB length and improve cathode performance. An ionic conducting path can be created by introducing a second phase with high ionic conductivity to form a composite electrode [8–11]. Alternatively, an ionic conducting path can be produced by tailoring the composition of single-phase electrodes to introduce oxygen vacancies into the lattice [12,13]. Many mixed oxygen-ionic and electronic conducting oxides have been developed and investigated as potential cathode materials of intermediate temperature (IT) SOFCs [14–18].

Over the past several years, $LnBaCo_2O_{5+\delta}$ has become one of the most desirable types of single-phase cathode materials for intermediate temperature (IT) SOFCs [19–25]. These oxides possess a lattice structure related to perovskite, where ordered A-site cations ($Ln^{3+}$ and $Ba^{2+}$) and oxygen vacancies are localized into layers. The ideal structure of these compounds can be represented by the stacking sequence $|LnO_\delta|CoO_2|BaO|CoO_2$, which is based on the structure of cubic perovskite. The transformation of a simple cubic perovskite with randomly occupied A sites into a layered crystallite with alternating lanthanide and alkaline-earth planes reduces the strength of oxygen bonding and provides disordered free channels for ionic motion. Therefore, the oxygen in $LnO_\delta$ and BaO layers displays high diffusivity, and electron transport in $CoO_2$ layers is facile. As a result, selected materials display both high ionic and electronic conductivity. Furthermore, these materials may also show high surface

* Corresponding author. Tel.: +86 25 83172256; fax: +86 25 83172256.
E-mail address: shaozp@njut.edu.cn (Z. Shao).
URL: http://shaogroup.njut.edu.cn (Z. Shao).

exchange kinetics at a reduced temperature [26,27]. Recent investigations from different groups have demonstrated that $LnBaCo_2O_{5+\delta}$ cathodes perform well in IT-SOFCs [19–25].

Among the various $LnBaCo_2O_{5+\delta}$ oxides, PrBC has received a considerable amount of attention due to its high surface exchange kinetics and bulk diffusion rate [26,28–34]. Recently, we applied a PrBC cathode in reduced temperature SOFCs with an oxygen-ion-conducting samaria-doped ceria electrolyte or a proton-conducting electrolyte [28–31]. A peak power density (PPD) as high as $620\,mW\,cm^{-2}$ with an anode-supported thin-film SDC electrolyte fuel cell and a PrBC cathode and an interfacial polarization resistance as low as $0.4\,\Omega\,cm^2$ based on symmetric two-electrode cells were achieved at 600 °C [28]. The high thermal expansion coefficient (TEC) of PrBC is a significant limitation and is common in cobalt-based perovskite oxides. A second ion-conducting phase composed of the same material as the electrolyte has been added to electrode materials such as LSM, $La_{0.6}Sr_{0.4}Co_{0.2}Fe_{0.8}O_{3-\delta}$ (LSCF) and $Sm_{0.5}Sr_{0.5}CoO_{3-\delta}$ (SSC) to produce a composite electrode that is thermo-mechanically compatible with the electrolyte. Typically, the introduction of a proper amount of a highly conductive second phase to an electrode with poor ionic conductivity significantly increases electrode performance. However, the effect of composite formation on the electrode performance of PrBC cathodes is controversial. For example, Zhu et al. reported a significant improvement in electrode performance by introducing a proper amount of SDC as second phase [33], while Zhou et al. reported a slight increase in cathodic ASR based on a symmetrical cell test [34]. Thus, further investigation of the performance of PrBC + SDC composite electrodes is necessary.

In this study, PrBC was synthesized and investigated as a cathode in IT-SOFCs containing an SDC electrolyte. SDC was introduced as the second phase to form a composite electrode with PrBC by a conventional mechanical mixing technique. The effect of weight ratio of SDC on the thermal expansion behavior and electrode performance was systematically investigated and an explanation for improved electrode performance was proposed.

## 2. Experimental

### 2.1. Synthesis and fabrication

PrBC and SDC oxide powders were prepared by a combined EDTA-citrate complexing sol–gel process. A detailed procedure for the preparation of PrBC and SDC was reported in a previous publication [35]. Composite oxides of PrBC + SDC were prepared by high energy ball milling (Pulverisette 6) of PrBC (calcined at 950 °C) and SDC powder (calcined at 850 °C) in ethanol liquid media for half an hour.

SDC electrolytes for symmetric cell and three-electrode cell fabrication were prepared by dry pressing and high-temperature sintering (1450 °C). To prepare two-electrode symmetric cells, cathode materials were dispersed into a solution of EG, ethanol and isopropyl alcohol. The resultant slurry was symmetrically deposited onto both surfaces of the electrolyte by an air-drive spray technique and was fired at 1000 °C in air for 2 h. To prepare three-electrode cells, a slurry of the composite cathode was deposited on one side of a SDC electrolyte with an area of $0.26\,cm^2$ and was fired at 1000 °C in air for 2 h. The resultant electrode was used as a working electrode (WE) in a three-electrode cell. To obtain the counter electrode (CE), a Pt electrode with the same shape as the WE was deposited on the other side of the SDC electrolyte and was fired at 900 °C in air for 30 min. To obtain the reference electrode (RE), a silver electrode was encircled around the CE, maintaining a 4 mm gap.

Anode-supported dual-layer cells with a thin-film SDC electrolyte were fabricated via dual dry pressing [28]. A green anode pellet was obtained by pressing pre-mixed NiO and SDC powder at a 60:40 weight ratio with a 15-mm stainless steel die. To form a dual-layer pellet, a specific amount of SDC powder was dispersed homogeneously over the open surface of the green anode pellet and was pressed with the aforementioned die. The resultant dual-layer pellets were sintered at 1450 °C for 5 h in air. A suspension of cathode material was spray-deposited over the electrolyte surface and was fired at 1000 °C in air for 2 h to form complete cells with an effective cathode geometric surface area of $0.48\,cm^2$.

### 2.2. Basic characterization

Rectangular-shaped bars with dimensions of $2\,mm \times 5\,mm \times 12\,mm$ were sintered at 1100 °C for 5 h in air and were used for TEC and electrical conductivity measurements. TECs of sintered samples were measured using a Netzsch DIL 402C dilatometer at temperatures between 30 and 900 °C at a heating rate of $5\,°C\,min^{-1}$ in air. Electrical conductivity was measured according to a four-probe DC method. Two silver wires were used as current leads, while a second set of silver wires were attached to the electrodes and used as voltage probes. A constant current was created between the two current wires, and the voltage was recorded by a Keithley 2420 source meter. The data acquisition and instrument control were performed by Labview (National instrument) software. Measurements were performed between 900 and 300 °C at 10 °C decrements, where a cooling rate of $5\,°C\,min^{-1}$ was employed. At each temperature, sufficient time was allowed for the conductivity stabilization. Conductivity was calculated by the following relationship:

$$\sigma = \frac{1}{R} \times \frac{l}{S} \tag{1}$$

where $l$, $S$ and $R$ represent the length, cross-sectional area and DC resistance, respectively.

In oxygen temperature-programmed desorption ($O_2$-TPD) experiments, 0.15 g of powdered sample with a mesh size of 40–60 was placed into a U-type quartz reactor with an inner diameter of 3 mm. High-purity helium (>99.999%) was fed into the reactor at a rate of $15\,ml\,min^{-1}$ (STP). After circulating helium gas at room temperature for half an hour to remove any weakly adsorbed species, the reactor was heated to a final temperature of 930 °C at a rate of $10\,°C\,min^{-1}$. During the heating process, helium transported oxygen molecules, which released from the oxide lattice, to a mass spectrometer (Hiden, QIC-20) for on-line oxygen concentration analysis.

### 2.3. Electrochemical characterization

Electrochemical impedance spectroscopy (EIS) was performed with a Solartron 1260 frequency response analyzer and a Solartron 1287 potentiostat. Impedance measurements were conducted between $10^{-1}$ and $10^5$ Hz, where an ac signal amplitude of 10 mV and zero dc bias were applied. The area specific resistance of the electrode was determined from EIS. The oxygen partial pressure of the atmosphere during EIS measurements was controlled at 0.04–1 atm by mixing $O_2$ and $N_2$ with mass flow controllers. The overall impedance data were collected with ZPlot 2.9c software program and fitted by a complex non-linear least squares (CNLS) fitting program within ZView 2.9. Cathodic overpotential was measured using a Solartron 1287 potentiostat/galvanostat and Corrware 2.9 c software. The IR drop, originating from the electrolyte and lead/contact resistances, was combined with EIS data to establish IR-free $I/E$ data.
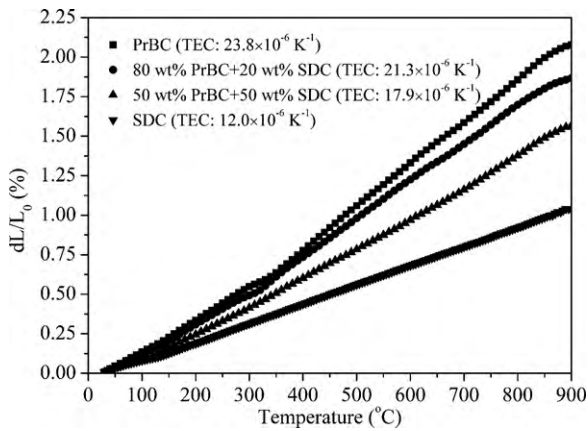
**Fig. 1.** Thermal expansion curves of SDC, PrBC, 80 wt% PrBC + 20 wt% SDC, and 50 wt% PrBC + 50 wt% SDC composites at 30–900 °C in air, with a heating rate of 5 °C min$^{-1}$.

### 2.4. I–V polarization test

The performance of composite cathodes was evaluated in complete cells at an in-lab SOFC test station. To obtain a fuel cell reactor, the cell was attached to one end of a quartz tube with the anode inside by using silver for sealing. Humidified hydrogen was fed into the anode at a flow rate of 80 ml min$^{-1}$, while oxygen in ambient air was fed to the cathode. A thermocouple was positioned near the surface of the cathode to monitor and control the temperature. *I–V* polarization tests were based on a four lead configuration and were measured with a digital source meter (Keithley 2420).

## 3. Results

### 3.1. Thermal expansion coefficient

Fig. 1 shows the thermal expansion curves of SDC, pure PrBC, 80 wt% PrBC + 20 wt% SDC and 50 wt% PrBC + 50 wt% SDC composites at 30–900 °C in air atmosphere and a heating rate of 5 °C min$^{-1}$. All thermal expansion curves showed a gradual increase in d$L$/$L_0$ with an increase in temperature. In a single-phase SDC pellet, linear thermal expansion curves were observed over the entire temperature range (30–900 °C). However, the thermal expansion curves of PrBC revealed an obvious change in slope around 300 °C. Similar results were also observed for 80 wt% PrBC + 20 wt% SDC composites, while a change in slope was less obvious in curves derived from 50 wt% PrBC + 50 wt% SDC composites.

The average TEC of each sample was derived from thermal expansion data. Results indicated that the TEC of SDC was 12.0 × 10$^{-6}$ K$^{-1}$ between 30 and 900 °C, which is similar to the TEC reported by Pikalova et al. (12.3 × 10$^{-6}$ K$^{-1}$) [36]. Pure PrBC possessed a TEC of 23.8 × 10$^{-6}$ K$^{-1}$ between 30 and 900 °C, which is similar to the results of Zhou et al., who reported a TEC of 21.5 × 10$^{-6}$ K$^{-1}$ [34]. A high TEC is frequently observed for cobalt-rich perovskite oxides such as Ba$_{0.5}$Sr$_{0.5}$Co$_{0.8}$Fe$_{0.2}$O$_{3-\delta}$ (BSCF) [37] and SSC [38].

Compared to pure PrBC, the introduction of SDC into PrBC led to a decrease in TEC. Specifically, higher amounts of SDC caused a decrease in the TEC, while a TEC of 21.3 and 17.9 × 10$^{-6}$ K$^{-1}$ was observed for 80 wt% PrBC + 20 wt% SDC and 50 wt% PrBC + 50 wt% SDC composites, respectively. Furthermore, the TEC of composite electrodes were fitted to the following equation:

$$TEC_{Composite\ (y\%A+(1-y\%)B)} = y\%TEC_A + (1 - y\%)TEC_B \quad (2)$$

where $y$, $A$ and $B$ denote the volume fraction, PrBC and SDC, respectively.



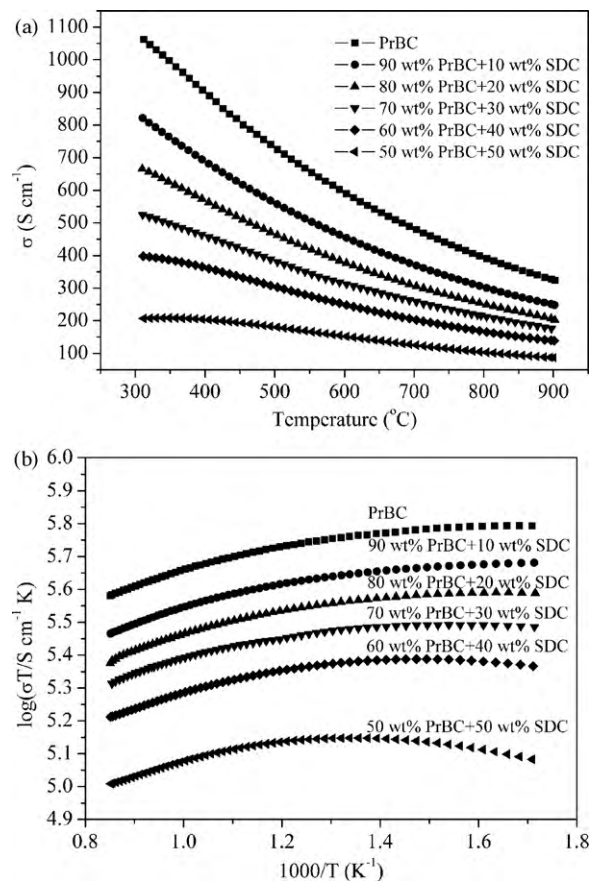**Fig. 2.** Temperature dependence of DC conductivities for PrBC and PrBC + SDC composites with various amounts of SDC between 300–900 °C in air.

### 3.2. DC conductivity

For practical applications, the electrode materials should possess sufficient electrical conductivity to ensure efficient current collection and to minimize contact resistance, especially under a high polarization current density. Fig. 2a shows the DC conductivity of PrBC and various PrBC + SDC composites with various amounts of SDC between 300 and 900 °C. The total conductivity of pure PrBC was between 1065 S cm$^{-1}$ (900 °C) and 320 S cm$^{-1}$ (300 °C), which is comparable to the results reported in the literature [34]. A linear decrease in conductivity with a decrease in temperature was also observed, suggesting that PrBC displays conduction behavior similar to metals.

By introducing SDC as a second phase, a drop in electrical conductivity was observed, where higher amounts of SDC resulted in a decrease in conductivity. For example, the total conductivity at 600 °C was 590, 454, 377, 312, 248 and 152 S cm$^{-1}$ for PrBC and PrBC + SDC composites containing 90, 80, 70, 60 and 50 wt% SDC, respectively. However, even 50 wt% PrBC + 50 wt% PrBC composites displayed high conductivity, which reached approximately 200 S cm$^{-1}$ at 300 °C and 90 S cm$^{-1}$ at 900 °C, as shown in Fig. 2a. Moreover, the effect of temperature on electrical conductivity was less prominent with an increase in SDC content. In Fig. 2b, electrical conductivity data are presented as a plot of log($\sigma T$) vs. 1000/$T$. The results clearly indicate a change in the temperature dependence of electrical conductivity with an increase in SDC content.
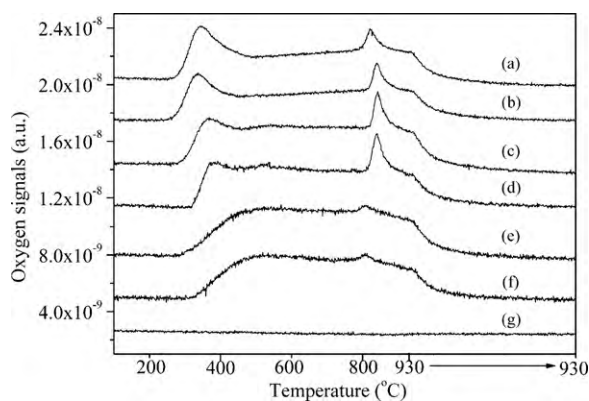
**Fig. 3.** O$_2$-TPD profiles of PrBC (a), 90 wt% PrBC + 10 wt% SDC (b), 80 wt% PrBC + 20 wt% SDC (c), 70 wt% PrBC + 30 wt% SDC (d), 60 wt% PrBC + 40 wt% SDC (e), 50 wt% PrBC + 50 wt% SDC (f) and SDC (g), calcined at 1100 °C for 5 h.

### 3.3. O$_2$-TPD

O$_2$-TPD is a facile and effective technique for the analysis of bulk oxygen mobility and surface oxygen activity of the oxide. In a typical O$_2$-TPD experiment, the sample is programmatically heated in a flowing inert atmosphere, resulting in the thermal reduction of cobalt in the oxide lattice and a subsequent release of oxygen. The release of oxygen from the oxide involves both bulk diffusion and surface reactions. The shape of the O$_2$-TPD profile is closely related to the bulk and surface properties of the oxide. Fig. 3 shows the O$_2$-TPD profiles of PrBC and PrBC + SDC composites with various amounts of SDC, calcined at 1100 °C for 5 h. All peaks were normalized based on the amount of PrBC in the composite. For comparison, the O$_2$-TPD profile of SDC is also presented, where the dissociation of oxygen from SDC was not observed because cobalt oxides are not present in SDC. In pure PrBC oxide, oxygen was released in two temperature zones, where the first dissociation began at 300 °C and ended at approximately 500 °C, while the second release began at 800 °C. These two peaks were identified as the α peak and β peak, respectively. A progressive change in the shape of the α peak and β peak was observed with an increase in SDC content.

### 3.4. Symmetric two-electrode measurement

Fig. 4 shows EIS data of PrBC and PrBC + SDC composites at 600 °C in air under open circuit voltage (OCV) conditions. For a more clear
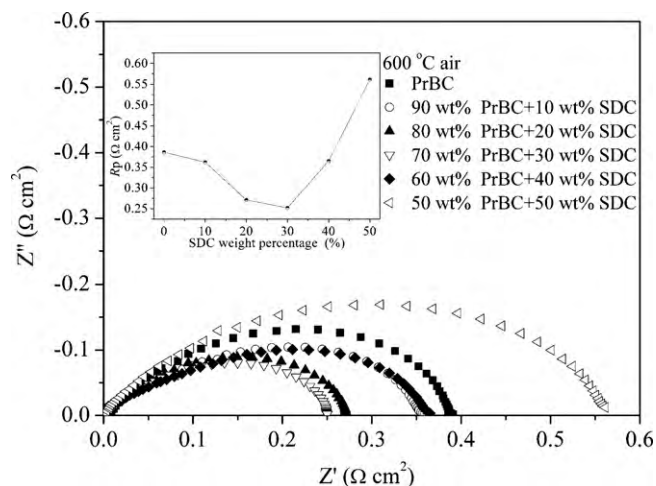


**Fig. 4.** Typical EIS of PrBC and PrBC + SDC composites at 600 °C in air under open circuit conditions.

comparison, the ohmic resistance of cells was eliminated in the EIS. The difference between the axis intercepts of the EIS plot can be considered the electrode polarization resistance ($R_p$). EIS plots clearly indicate that the SDC content had a significant effect on the electrode polarization resistance of the electrodes, where the calculated values are shown in Fig. 4. The $R_p$ decreased with an increase in SDC content, reached a minimum at a SDC content of 30% and increased sharply with a further increase in SDC. The polarization resistances were 0.386, 0.362, 0.271, 0.252, 0.365 and 0.561 $\Omega$ cm$^2$ for PrBC and PrBC + SDC composites containing 0, 10, 20, 30, 40 and 50 wt% SDC, respectively.

Fig. 5 shows the EIS of various PrBC + SDC composite electrodes at 600 °C under selected atmospheres, where the $pO_2$ varied from 0.04 to 1 atm. As shown in Fig. 5f, the equivalent circuit L–$R_{ohm}$–($R_{E1}$–CPE1)–($R_{E2}$–CPE2) was adopted to fit EIS data. L corresponded to the high-frequency induction tail caused by the device and leads, $R_{ohm}$ was the ohmic resistance of the cell and ($R_{E1}$–CPE1) and ($R_{E2}$–CPE2) corresponded to the high and low arcs, respectively. The solid lines in Fig. 5 are the fitted curves by using the aforementioned equivalent circuit, while the points indicate experimental data. The impedance data and fitted curves were in good agreement, which suggests that the equivalent circuit is an appropriate approximation for both single-phase and composite cathodes.

Fig. 6 presents the $R_{E1}$ and $R_{E2}$ of PrBC and the various PrBC + SDC composite electrodes, derived from Fig. 5, as a function of the oxygen partial pressure at 600 °C in Arrhenius plots. The results indicate that the slope of $\ln(1/R_{E1})$ vs. $\ln(pO_2)$ was between 0.18 and 0.20, while the slope of $\ln(1/R_{E2})$ and $\ln(pO_2)$ was between 0.33 and 0.40 for PrBC and PrBC + SDC electrodes. In general, each elemental process displays a unique dependence on the $pO_2$, where a value of 0.25 usually corresponds to a charge transfer process and a value of 0.5 corresponds to surface diffusion [39]. Based on the aforementioned results and previous observations of PrBC electrodes [28], the high-frequency arc was likely associated with charge transfer processes, while the low frequency arc was associated with surface diffusion. As shown in Fig. 2, PrBC is highly conductive; thus, $R_{E1}$ was less likely due to electron charge transfer process while $R_{E1}$ may be a result of oxygen-ion charge transfer process.

The results shown in Fig. 7 analyzed to determine the effect of SDC content on the $R_{E1}$ and $R_{E2}$ of PrBC + SDC composite electrodes. In general, $R_{E1}$ decreased monotonously with an increase in SDC content. As to $R_{E2}$, it decreased slightly with an increase in SDC amount at low SDC content until it reached 20–30 wt%, then the $R_{E2}$ increased sharply with the further increase in SDC content. A similar trend was observed at all investigated oxygen partial pressures. Clearly, the best performance achieved for the PrBC + SDC composite electrode containing 30 wt% SDC is due to both small $R_{E1}$ and $R_{E2}$, while the large $R_p$ at high SDC content is mainly due to the sharp increase in $R_{E2}$.

### 3.5. Three-electrode measurement

Cathodic overpotential is an important component of electrode performance. To further investigate the effect of SDC content on electrode performance, three-electrode cells were constructed and cathodic polarization analysis was performed on PrBC + SDC composite electrodes. Fig. 8 presents the IR-corrected Tafel plots of PrBC + SDC composite electrodes with various amounts of SDC at 600 °C in air. The cathodic overpotential decreased with an increase in SDC and reached a minimum at 30 wt% SDC. A further increase in SDC content caused an increase in the cathodic overpotential. A similar trend was observed in the symmetric cell test. At an overpotential of −0.15 V, the current density was approximately 198, 344, 430, 174 and 110 mA cm$^{-2}$ for PrBC + SDC composite electrodes with a SDC content of 10, 20, 30, 40 and 50 wt%, respectively.
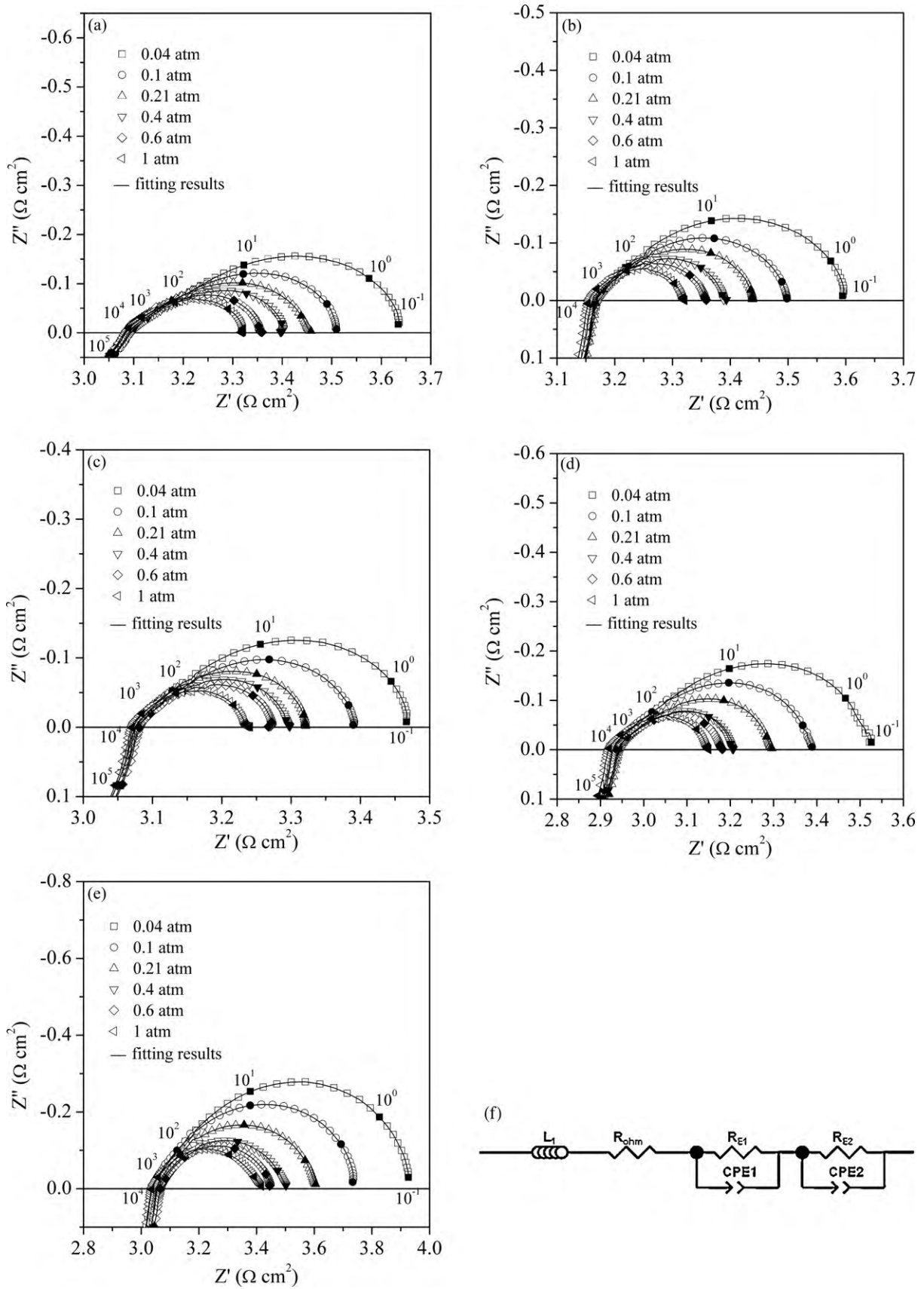
**Fig. 5.** Nyquist plots of EIS data obtained from symmetrical two-electrode cells measured under open circuit voltage conditions with oxygen partial pressure from 0.04 to 1 atm at 600 °C. Cells contained composite electrodes with 90 wt% PrBC + 10 wt% SDC (a), 80 wt% PrBC + 20 wt% SDC (b), 70 wt% PrBC + 30 wt% SDC (c), 60 wt% PrBC + 40 wt% SDC (d) and 50 wt% PrBC + 50 wt% SDC (e). Equivalent circuits (f) adopted for fitting EIS data.
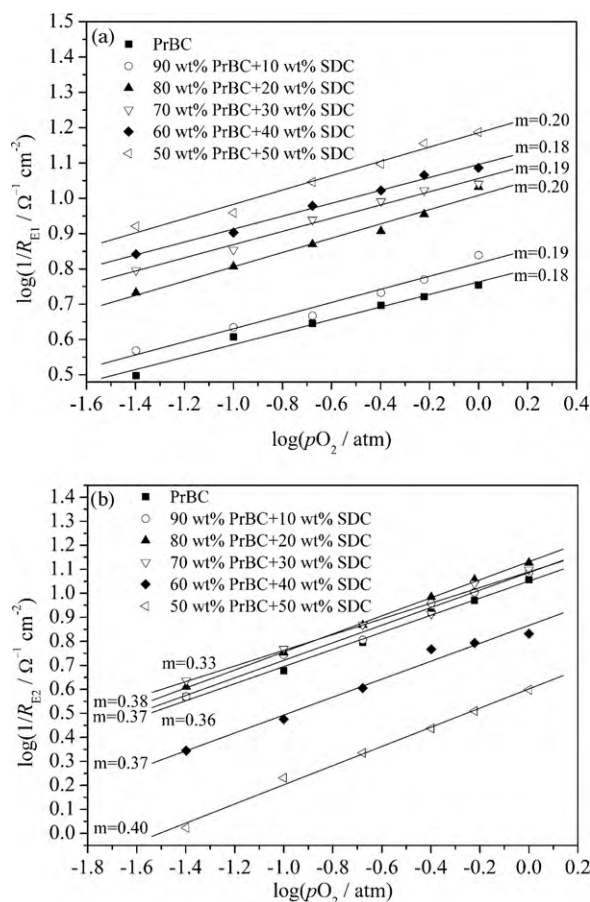
**Fig. 6.** Arrhenius plots of $R_{E1}$ and $R_{E2}$ from PrBC and PrBC + SDC composite electrodes as a function of oxygen partial pressure at 600 °C.



**Fig. 7.** Effect of SDC content on $R_{E1}$ and $R_{E2}$ of PrBC + SDC composite electrodes.

The exchange current density, $i_0$, is a direct reflection of the intrinsic electrocatalytic activity and was calculated according to the Bulter–Volmer equation:

$$i = i_0 \left[ exp\left(\frac{\alpha_a F\eta}{RT}\right) - exp\left(\frac{-\alpha_c F\eta}{RT}\right) \right] \qquad (3)$$

In high field overpotential, the anodic reaction can be ignored and $i_0$ can be obtained from the $y$-intercept of a plot of $\log i$ vs. $\eta$. Thus, $i_0$ was calculated according to the following equation:

$$\mathrm{Log}\, i = \mathrm{Log}\, i_0 - \frac{\alpha_c nF}{2.303RT}\eta \qquad (4)$$

where $\eta$ is the cathodic overpotential and $\alpha_c$ is the cathodic coefficient, $n$ is the total number of transferred electrons, $F$ is the Faraday constant, $R$ is the gas constant and $T$ is the absolute temperature.

The cathodic coefficient can be calculated by:

$$\alpha_c = \frac{\gamma}{\nu + r\beta}$$

where $\gamma$, $r$ and $\beta$ are the number of electrons transferred before the rate limiting step, the number of electrons transferred during the rate limiting step, and the symmetry coefficient (typically assumed to be 0.5), respectively.

The $i_0$ of PrBC + SDC composite electrodes with a SDC content of 10, 20, 30, 40 and 50 wt% was approximately 65, 114, 200, 55 and 35 mA cm$^{-2}$, respectively. Again, the composite electrode containing 30 wt% SDC showed the highest exchange current density.
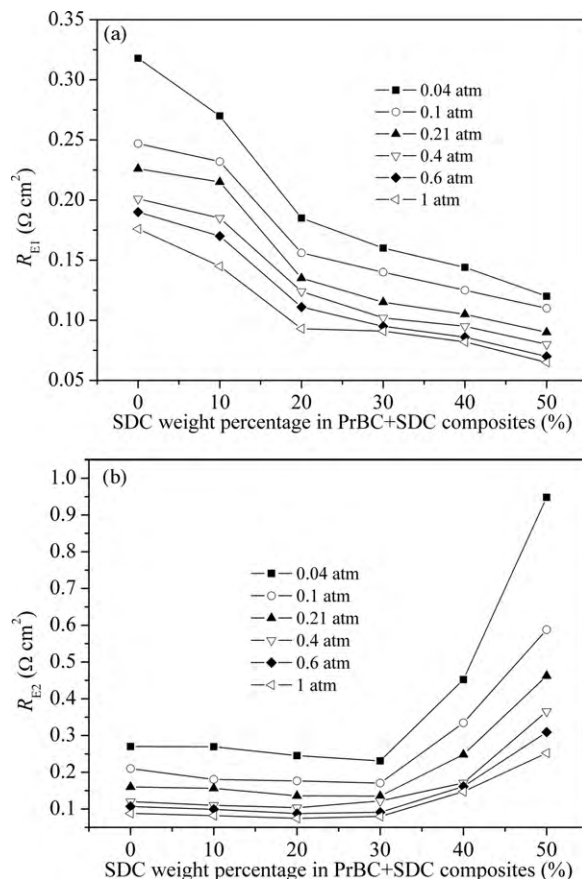
### 3.6. Single cell performance

The electrochemical performance of the various electrodes was further investigated in a complete cell. Anode-supported cells with a Ni + SDC anode, a thin-film SDC electrolyte (approximately 25 μm) and PrBC + SDC cathodes were fabricated. Fig. 9 shows the peak power densities (PPD), power densities at 0.7 V (0.7PD) and shorted current densities (SCD) of cells with different cathodes at 600 °C. A PPD and 0.7PD of 620 and 400 mW cm$^{-2}$ was achieved with a pure PrBC cathode. The PPD and 0.7PD increased progressively with an increase in SDC content until the concentration of SDC reached 30 wt%. The cell containing a composite cathode com-
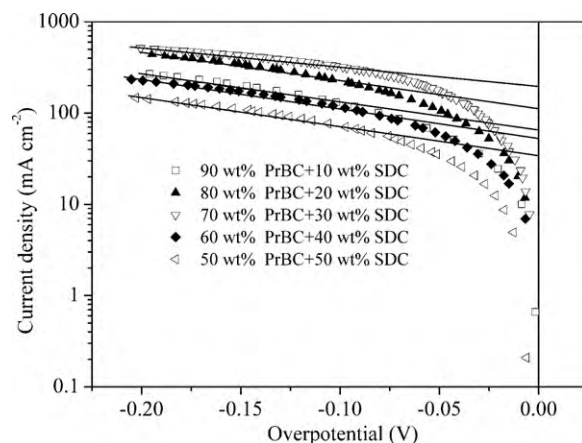


**Fig. 8.** IR-corrected Tafel plots of PrBC + SDC composite electrodes with various amounts of SDC at 600 °C in air.
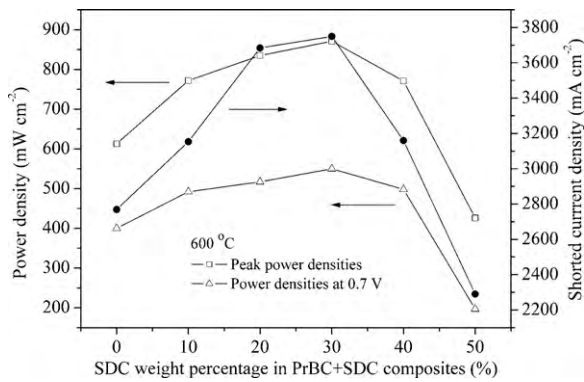
**Fig. 9.** Peak power densities, power densities at 0.7 V and shorted current densities of cells with different PrBC + SDC composite electrodes at 600 °C.

posed of 70 wt% PrBC + 30 wt% SDC delivered a PPD of 875 mW cm$^{-2}$ at 600 °C, which is comparable to a similar cell with a BSCF electrode [5]. However, a composite electrode with a greater SDC content led to decreased cell performance. For example, the PPD and 0.7PD of a fuel cell with a 50 wt% PrBC + 50 wt% SDC composite cathode was only 425 and 197 mW cm$^{-2}$, which is even lower than a cell with a pure PrBC cathode. Except for the composition of the cathode, all cell materials and fabrication processes were identical in each cell; thus, significant differences in cell performance were due to the performance of the cathode. The observed trend in single cell performance matched the electrochemical performance of PrBC + SDC composite electrodes in a symmetric cell test and three-electrode overpotential test.
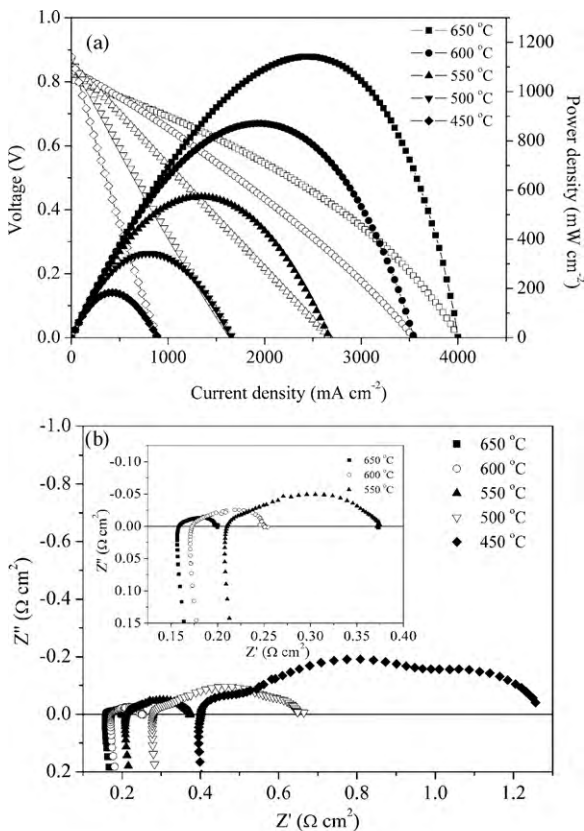


**Fig. 10.** I–V and I–P curves of a cell with 70 wt% PrBC + 30 wt% SDC composite cathode at various temperatures (a) and the corresponding cell impedance of a single cell measured at OCV conditions (b).

Fig. 10 shows the I–V and I–P curves of the cell containing a 70 wt% PrBC + 30 wt% SDC cathode at various temperatures. A PPD of 1150 mW cm$^{-2}$ was achieved at 650 °C. The corresponding cell impedance of the single cell at OCV conditions is shown in Fig. 10b. At 650 °C, the ohmic resistance of the cell was approximately 0.1 Ω cm$^2$, while the electrode polarization resistance of the cell was 0.05 Ω cm$^2$. At 550 °C, the electrode polarization resistance (0.16 Ω cm$^2$) was still lower than the ohmic resistance of the cell (0.215 Ω cm$^2$). The electrode polarization resistance began to play a dominant role in total cell resistance at 450 °C.

## 4. Discussion

### 4.1. Thermal expansion behavior

The thermal expansion of oxygen deficient perovskites can be contributed to two phenomena; actual thermal expansion created by atomic vibration of the lattice or chemical expansion associated with a change in valence and spin state of the cations. In connection with O$_2$-TPD results in Fig. 3, thermal expansion at temperatures less than 300 °C (before the change in slope) was caused by atomic vibrations of the lattice. The dramatic increase in thermal expansion after the change in slope was a result of chemical expansion due to the generation of oxygen vacancies and changes in the spin or/and oxidation state of B-site cations (cobalt).

It has been reported that a physical mixture of two compounds with different TECs results in a composite TEC that is a volumetric average of the constituent materials [40]. However, phase reactions between components may alter thermal expansion behavior [41]. Previously, we demonstrated that a phase reaction between PrBC and SDC does not occur at temperatures up to 1100 °C [28]. Furthermore, the TEC of composites was equal to the volumetric average of PrBC and SDC, which further supported a lack of phase reactions between PrBC and SDC in the composites. Thus, an increase in SDC content results in a reduced TEC and produces an electrode that is thermo-mechanically compatible with a SDC electrolyte.

### 4.2. Electrode performance

The introduction of a highly ionic conductive second phase and subsequent formation of a composite electrode is frequently conducted to improve electrode performance at reduced temperatures. For example, the introduction of YSZ or GDC to LSM to obtain LSM + YSZ/GDC composites can significantly increase electrode performance between 650 and 850 °C as compared to pure LSM [8,42]. It is believed that the creation of ionic diffusion paths within the bulk of the electrode is the main cause for such obvious improvement in electrode performance. The creation of ionic conduction paths within the interior of the electrode extends the active sites of oxygen reduction from the traditional TPB region to the entire exposed surface of the cathode. This theory also explains the improved performance of LSCF + SDC and SSC + SDC composite cathodes compared to pure LSCF or SSC electrodes at reduced temperatures. It is well known that LSCF and SSC are mixed conductors and possess considerable ionic conductivity at elevated temperatures. However, at temperatures lower than 650 °C, the ionic conductivity of LSCF and SSC is negligible. The introduction of a second phase containing SDC, which has a reported ionic conductivity of approximately 10$^{-2}$ S cm$^{-1}$ at 600 °C, can effectively increase the apparent conductivity of the electrode and improve cell performance.

GdBaCo$_2$O$_{5+\delta}$ (GdBC) has an ionic conductivity of 10$^{-2}$ S cm$^{-1}$ at 500 °C [27], which is comparable to SDC at 600 °C. Moreover, greater bulk diffusion is observed in PrBC than GdBC [26], which indicates that PrBC has a higher ionic conductivity than SDC at
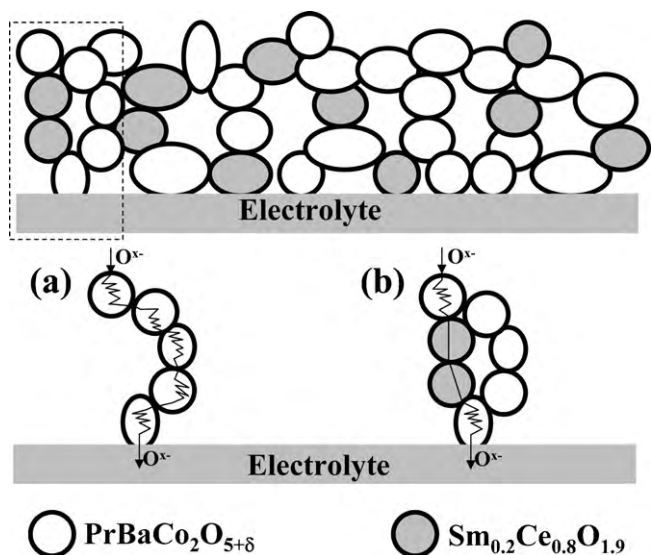
**Fig. 11.** Schematic shows of oxygen-ion diffusion paths in a pure PrBC cathode (a) and a PrBC + SDC composite cathode (b).

intermediate-to-low temperatures. The enhanced performance of PrBC + SDC composite electrodes cannot be fully explained by the creation formation of ionic conduction paths. Indeed, we previously demonstrated that the performance of BSCF + SDC composite electrodes was not significantly improved compared to pure BSCF electrodes because pure BSCF is a good ionic conductor at reduced temperatures [43].

$LnBaCo_2O_{5+\delta}$ double perovskite oxides are one-dimensional materials with respect to oxygen diffusion, where fast oxygen diffusion channels exist only in the $LnO_\delta$ planes. Alternatively, the oxygen diffusion rate perpendicular to $LnO_\delta$ planes is negligible [27,44,45]. Under the experimental conditions, $LnBaCo_2O_{5+\delta}$ was polycrystalline and was composed of many small crystals in a random orientation. The polycrystalline structure and one-dimensional oxygen diffusion characteristics of PrBC could result in a tortuous path for oxygen diffusion. Therefore, the apparent ionic conductivity of polycrystalline $LnBaCo_2O_{5+\delta}$ cathodes may be significantly lower than the conductivity of the single crystal. Indeed, we demonstrated that a ceramic membrane composed of polycrystalline PrBC displayed a lower oxygen permeation flux than a BSCF membrane, which possesses a cubic perovskite structure and three-dimensional oxygen diffusion paths [31]. As shown in Fig. 5, the large $R_{E1}$ of polycrystalline PrBC electrodes clearly supported a relatively low apparent ionic conductivity.

Based on the above analysis, the improved performance of PrBC + SDC composites can be explained by the mechanism shown in Fig. 11. In a pure PrBC electrode, due to its polycrystalline structure, the oxygen diffusion path is very tortuous (Fig. 11a). As a result, porous polycrystalline PrBC electrodes possess relatively low oxygen conductivity, and the effective thickness of the active PrBC layer for oxygen reduction is relatively thin. Due to the relatively low ionic conductivity and high surface exchange kinetics of PrBC, the electrode polarization resistance of polycrystalline PrBC electrodes was contributed to oxygen-ion charge transfer processes and resulted in a $R_{E1}$ that was greater than $R_{E2}$. As shown in Fig. 11b, the introduction of an ionic conducting phase allowed SDC particles to connect PrBC grains, which shortened the path for ionic diffusion and extended the effective thickness of the active layer of the electrode for oxygen reduction. Thus, the introduction of a small amount of SDC (10–30 wt%) reduced $R_{E1}$ and $R_{E2}$; however, the reduction in $R_{E1}$ was greater than the reduction in $R_{E2}$. Clearly, an increase in SDC decreased the tortuosity of the oxygen diffusion

path and caused a monotonous decrease in the $R_{E1}$ associated with the charge transfer process, as shown in Fig. 7.

The sharp increase in $R_{E2}$ at SDC concentrations greater than 30 wt% may be explained by surface exchange kinetics. Although the introduction of SDC increased the apparent conductivity of the electrode, it also decreased the surface activity, as PrBC has much higher surface exchange kinetics than SDC. At high concentrations of SDC, a large area of the PrBC surface was likely covered by SDC, blocking oxygen diffusion, which can also be directly observed in $O_2$-TPD curves in Fig. 3. As a result, the polarization resistance associated with surface diffusion ($R_{E2}$) increased sharply with an increase in SDC concentration greater than 30 wt%.

## 5. Conclusions

The amount of SDC in PrBC + SDC composites has a significant effect on the thermal expansion coefficient, total conductivity, oxygen release rate, oxygen-ion conduction in the electrode and oxygen diffusion at the surface of PrBC. The introduction of SDC into PrBC reduced the TEC and electrical conductivity of the electrodes. However, even at SDC concentrations as high as 50 wt%, the total conductivity of the composite remained high, and the composite electrodes could be successfully used as cathodes in SOFCs. By adopting a 70 wt% PrBC + 30 wt% SDC composite electrode, a low area specific resistance of only $0.25\,\Omega\,cm^2$ was achieved at $600\,^{\circ}C$, which is smaller than the resistance of pure PrBC electrodes. The improved performance of PrBC + SDC composite electrodes is due to an increase in the apparent oxygen-ionic conductivity. With an anode-supported thin-film electrolyte cell containing a 70 wt% PrBC + 30 wt% SDC composite electrode, a peak power density of 1150 and $573\,mW\,cm^{-2}$ was successfully achieved at 650 and $550\,^{\circ}C$, respectively. These exciting results indicate that PrBC-based composite electrodes can be applied to reduced-temperature SOFCs.

## References

[1] N.Q. Minh, J. Am. Ceram. Soc. 76 (1993) 563–588.
[2] S.C. Singhal, K. Kendall, High Temperature Solid Oxide Fuel Cells: Fundamentals, Design and Applications, Elsevier Advanced Technology, Oxford, 2003.
[3] N.P. Brandon, S. Skinner, B.C.H. Steele, Annu. Rev. Mater. Res. 33 (2003) 183–213.
[4] B.C.H. Steele, A. Heinzel, Nature 414 (2001) 345–352.
[5] Z.P. Shao, S.M. Haile, Nature 431 (2004) 170–173.
[6] J.P.P. Huijsmans, F.P.F. van Berkel, G.M. Christie, J. Power Sources 71 (1998) 107–110.
[7] M. Mogensen, S. Skaarup, Solid State Ionics 86–88 (1996) 1151–1160.
[8] E.P. Murray, S.A. Barnett, Solid State Ionics 143 (2001) 265–273.
[9] J.D. Kim, G.D. Kim, J.W. Moon, Y.I. Park, W.H. Lee, K. Kobayashi, M. Nagai, C.E. Kim, Solid State Ionics 143 (2001) 379–389.
[10] T.Z. Sholklapper, H. Kurokawa, C.P. Jacobson, S.J. Visco, L.C. De Jonghe, Nano Lett. 7 (2007) 2136–2141.
[11] A. Barbucci, R. Bozzo, G. Cerisola, P. Costamagna, Electrochim. Acta 47 (2002) 2183–2188.
[12] P.Y. Zeng, Z.P. Shao, S.M. Liu, Z.P. Xu, Sep. Purif. Technol. 67 (2009) 304–311.
[13] L.W. Tai, M.M. Nasrallah, H.U. Anderson, D.M. Sparlin, S.R. Sehlin, Solid State Ionics 76 (1995) 259–271.
[14] S. Bebelis, N. Kotsionopoulos, A. Mai, F. Tietz, J. Appl. Electrochem. 37 (2007) 15–20.
[15] W. Zhou, R. Ran, Z.P. Shao, J. Power Sources 192 (2009) 231–246.

[16] X.G. Zhang, M. Robertson, S. Yick, C. Deces-Petit, E. Styles, W. Qu, Y.S. Xie, R. Hui, J. Roller, O. Kesler, R. Maric, D. Ghosh, J. Power Sources 160 (2006) 1211–1216.
[17] H. Zhao, F. Mauvy, C. Lalanne, J.-M. Bassat, S. Fourcade, J.C. Grenier, Solid State Ionics 179 (2008) 2000–2005.
[18] F. Tietz, V.A.C. Haanappel, A. Mai, J. Mertens, D. Stöver, J. Power Sources 156 (2006) 20–22.
[19] Q.J. Zhou, T.M. He, Y. Ji, J. Power Sources 185 (2008) 754–758.
[20] A. Tarancón, A. Morata, G. Dezanneau, S.J. Skinner, J.A. Kilner, S. Estradé, F. Hernández-Ramírez, F. Peiró, J.R. Morante, J. Power Sources 174 (2007) 255–263.
[21] A. Tarancón, S.J. Skinner, R.J. Chater, F. Hernández-Ramírez, J.A. Kilner, J. Mater. Chem. 17 (2007) 3175–3181.
[22] H.T. Gu, H. Chen, L. Gao, L.C. Guo, Electrochim. Acta 54 (2009) 7094–7098.
[23] J.H. Kim, A. Manthiram, J. Electrochem. Soc. 155 (2008) B385–B390.
[24] A.M. Chang, S.J. Skinner, J.A. Kilner, Solid State Ionics 177 (2006) 2009–2011.
[25] J.H. Kim, Y. Kim, P.A. Connorb, J.T.S. Irvine, J. Bae, W.Z. Zhou, J. Power Sources 194 (2009) 704–711.
[26] G. Kim, S. Wang, A.J. Jacobson, L. Reimus, P. Brodersen, C.A. Mims, J. Mater. Chem. 17 (2007) 2500–2505.
[27] A.A. Taskin, A.N. Lavrov, Y. Ando, Appl. Phys. Lett. 86 (2005) 091910.
[28] D.J. Chen, R. Ran, K. Zhang, J. Wang, Z.P. Shao, J. Power Sources 188 (2009) 96–105.
[29] D.J. Chen, R. Ran, Z.P. Shao, J. Power Sources 195 (2010) 4667–4675.
[30] Y. Lin, R. Ran, C.M. Zhang, R. Cai, Z.P. Shao, J. Phys. Chem. A 114 (2010) 3764–3772.
[31] K. Zhang, L. Ge, R. Ran, Z.P. Shao, S.M. Liu, Acta Mater. 56 (2008) 4876–4889.
[32] G. Kim, S. Wang, A.J. Jacobson, Z. Yuan, W. Donner, C.L. Chen, L. Reimus, P. Brodersen, C.A. Mims, Appl. Phys. Lett. 88 (2006) 024103.
[33] C.J. Zhu, X.M. Liu, C.S. Yi, L. Pei, D.J. Wang, D.T. Yan, K.G. Yao, T.Q. Lu, W.H. Su, J. Power Sources 195 (2010) 3504–3507.
[34] Q.J. Zhou, F. Wang, Y. Shen, T.M. He, J. Power Sources 195 (2010) 2174–2181.
[35] H.X. Gu, R. Ran, W. Zhou, Z.P. Shao, J. Power Sources 172 (2007) 704–712.
[36] E.Y. Pikalova, V.I. Maragou, A.N. Demina, A.K. Demin, P.E. Tsiakaras, J. Power Sources 181 (2008) 199–206.
[37] W. Zhou, R. Ran, Z.P. Shao, W.Q. Jin, N.P. Xu, J. Power Sources 182 (2008) 24–31.
[38] H. Lv, Y.J. Wu, B. Huang, B.Y. Zhao, K.A. Hu, Solid State Ionics 177 (2006) 901–906.
[39] M.J. Escudero, A. Aguadero, J.A. Alonso, L. Daza, J. Electroanal. Chem. 611 (2007) 107–116.
[40] S.K. Pratihar, A. Dassharma, H.S. Maiti, J. Mater. Sci. 42 (2007) 7220–7226.
[41] F.M. Figueiredo, F.M.B. Marques, J.R. Frade, Solid State Ionics 138 (2001) 173–182.
[42] T. Tsai, S.A. Barnett, Solid State Ionics 93 (1997) 207–217.
[43] K. Wang, R. Ran, W. Zhou, H.X. Gu, Z.P. Shao, J. Ahn, J. Power Sources 179 (2008) 60–68.
[44] A. Maignan, C. Martin, D. Pelloquin, N. Nguyen, B. Raveau, J. Solid State Chem. 142 (1999) 247–260.
[45] C. Frontera, A. Caneiro, A.E. Carrillo, J. Oró-Solé, J.L. García-Muñoz, Chem. Mater. 17 (2005) 5439–5445.